PAPER

Check for updates

Heteropoly acid catalysts for limonene oxide isomerization: the correlation of catalyst acid strength to activity and selectivity†

Hyunju Lee,[a] Hsi-Hsin Lin[ab] and Brent H. Shanks [iD] *[ab]

Limonene extracted from plants and obtained from sugar fermentation can be converted into a broad range of chemicals for fuels, fragrances, pharmaceuticals, and novel polymers. A limonene oxide isomer, dihydrocarvone, has been widely used in the food, cosmetics, agrochemical, and pharmaceutical industries. Herein, acid strength effects on limonene oxide isomerization were investigated with a wide range of Brønsted acid catalysts using Keggin heteropoly acids (HPAs) and organosulfonic acids. Temperature-programmed desorption of 2,6-di-*tert*-butylpyridine (DTBP) was used to measure surface proton density and acid strength of the catalysts. A good correlation of surface acid strength represented by the DTBP desorption temperature with the turnover rate calculated using the amount of DTBP chemisorbed was obtained. Further, good correlations of acid strength, represented by desorption temperatures of ammonia and DTBP, to both the turnover rate and dihydrocarvone selectivity were established. This correlation held for the bulk and supported HPA catalysts and organosulfonic acid catalysts, thereby indicating that the turnover rate and dihydrocarvone selectivity are primarily determined by catalyst acid strength, regardless of the catalyst porosity and support surfaces. The findings not only provide an efficient strategy for upgrading a biomass derivative, limonene oxide, but also present an advancement in the selective characterization for Brønsted acid sites of HPA-type catalysts.
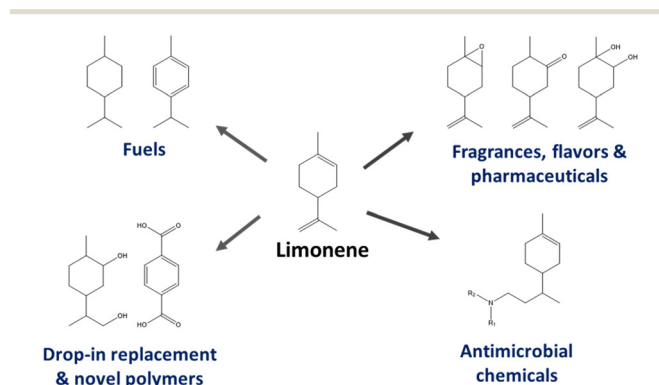
1. Introduction

Solid heteropoly acids (HPAs) are interesting catalytic materials due to their high Brønsted acidity and proton conductivity. HPAs, having the Keggin structure, are represented by the formula $H_{8-x}[X^{x+}M_{12}O_{40}]$ ($X = P^{5+}$ or Si^{4+}, $M = W^{6+}$ or Mo^{6+}). The acid strength of bulk HPAs depends on the elemental composition and is known to decrease in the order of $H_3PW_{12}O_{40}$ (HPW) > $H_4SiW_{12}O_{40}$ (HSiW) > $H_3PMo_{12}O_{40}$ (HPMo) > $H_4SiMo_{12}O_{40}$ (HSiMo).[1] They have been used in homogeneous and heterogeneous systems for a range of reactions including hydration, dehydration, condensation, esterification, alkylation, oxidation, *etc.*[2,3] As such, they have been identified as promising catalysts to valorize biomass and biomass-derived chemicals.[4,5]
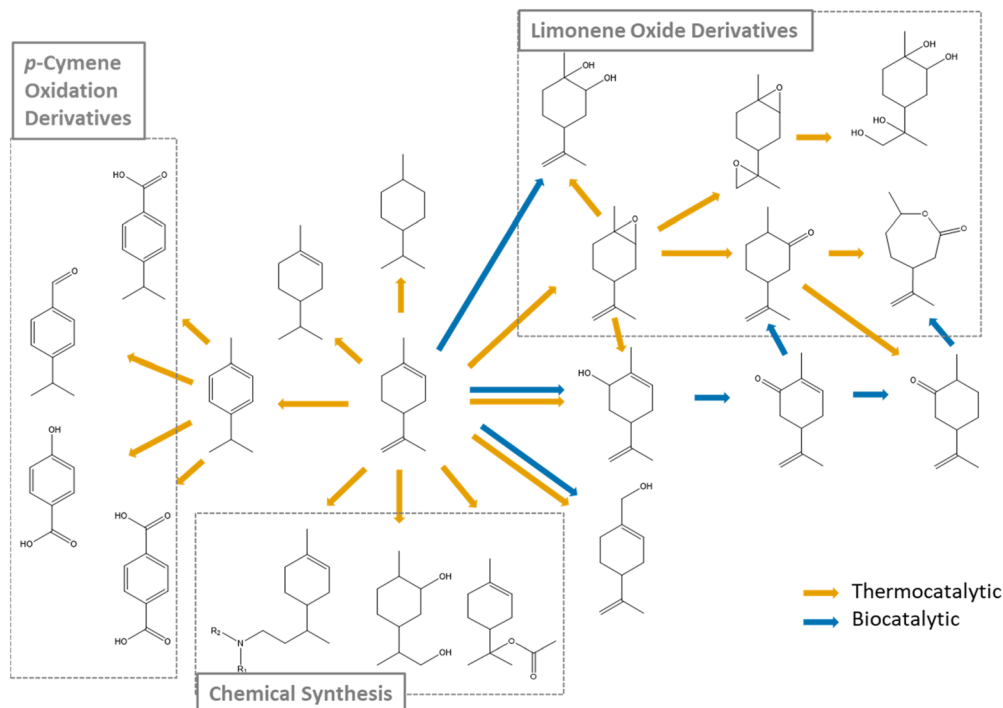
The conversion of biomass derivatives has been investigated to provide alternative options for petroleum-based chemicals and energy. Among various biomass-derived molecules, limonene has

received attention due to its versatility. Limonene is generally extracted from citrus peels such as waste orange rinds,[6,7] but it can also be produced through sugar fermentation[8] and waste tire pyrolysis.[9] Limonene production was valued at USD 1.45 billion globally in 2022 and is predicted to rise to USD 1.87 billion by 2028.[10] Notably, limonene has the attributes of a bioprivileged molecule in that it can be converted into a wide range of chemicals for use as fuels, fragrances, pharmaceuticals, and novel polymers, as shown in Scheme 1.[8,11–14] Through both chemical and biological pathways, a variety of molecules are accessible

[a] *Department of Chemical and Biological Engineering, Iowa State University, Ames, IA, 50011, USA. E-mail: bshanks@iastate.edu*
[b] *Center for Biorenewable Chemicals (CBiRC), Iowa State University, Ames, IA, 50011, USA*

† Electronic supplementary information (ESI) available. See DOI: https://doi.org/10.1039/d5cy00747j

Scheme 1 Applications of limonene-derived chemicals.

5318 | *Catal. Sci. Technol.*, 2025, **15**, 5318–5326

This journal is © The Royal Society of Chemistry 2025

Scheme 2 Limonene star diagram.

from limonene, as illustrated in a limonene "star" diagram (Scheme 2). For one branch of the diagram, limonene can be used as a precursor to oxidized derivatives with the same carbon skeleton as limonene including limonene oxide, perillyl alcohol, α-terpineol, carveol, carvone, and menthol.[9] A limonene oxide isomer, dihydrocarvone, is a valuable flavor and fragrance compound with a spearmint-like odor. It has been extensively used in the food (e.g., beverages, bakery product, candy), oral health (e.g., toothpaste), agrochemical (e.g., insect repellent), cosmetics (e.g., fragrance) and pharmaceutical industries.[15] Dihydrocarvone can also be used as an intermediate for producing antimalarial drugs[16] and chiral building blocks for ligands.[17] Its production from limonene oxide (Scheme 3) using acid[18–20] and Fe catalysts[21] was reported in previous studies with heteropoly acid catalysts showing good selectivity. As production of dihydrocarvone generally requires the use of solvents due to the high reactivity of limonene oxide in the presence of catalysts leading to oligomerization, the effects of the solvent on dihydrocarvone production has also been investigated.[18,19,21] However, systematic examination of the effects of catalytic properties has received little attention.
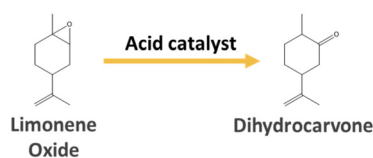
In this work, a wide range of acid catalysts in limonene oxide isomerization were investigated. Included were bulk and supported heteropoly acid catalysts (bulk HPW, bulk HPMo, HPW/SiO$_2$, HPW/TiO$_2$, and HPW/ZrO$_2$) as well as organosulfonic acid catalysts (Nafion NR50, propylsulfonic acid and arenesulfonic acid-functionalized silica). The primary goal was to examine the effect of catalyst acid strength on the reaction rate and selectivity. Temperature-programmed desorption (TPD) of 2,6-di-tert-butylpyridine (DTBP) was used to measure the surface proton concentration and acid strength of the catalysts in addition to typical ammonia TPD. These DTBP experiments were used to systematically characterize acid sites available for conversion of larger reactant molecules such as limonene oxide.

2. Experimental

2.1. Chemicals

All chemicals were used without further purification including phosphotungstic acid hydrate (Fisher), phosphomolybdic acid hydrate (Fisher), SiO$_2$ (Aerosil 300, Evonik), TiO$_2$ (P25, Sigma Aldrich), ZrO$_2$ (<100 nm, Sigma Aldrich), ethanol (Decon Laboratories), pluronic 123 (BASF), hydrochloric acid (HCl, 37.2 wt%, Sigma Aldrich), tetraethyl orthosilicate (TEOS, Alfa Aesar), (3-mercaptopropyl)trimethoxysilane (MPTMS, TCI America), H$_2$O$_2$ (30 wt%, Fisher), 2-(4-chlorosulfonylphenyl)ethyltrimethoxysilane (CSPTMS, 50% in toluene, Gelest), phenyltrimethoxysilane (PhTMS, TCI America), toluene (Fisher), dichloromethane (anhydrous, EDM Millipore), diethyl ether (Sigma Aldrich), Nafion NR50 (Alfa Aesar), sodium chloride (Fisher), tetramethylammonium chloride (TMACl, TCI America), sodium hydroxide standard solution (0.0100 M, Spectrum), limonene oxide (mixture of cis/trans-isomers with ratio of 0.74,

Scheme 3 Acid-catalyzed limonene oxide isomerization.

This journal is © The Royal Society of Chemistry 2025

Catal. Sci. Technol., 2025, 15, 5318–5326 | 5319

Sigma Aldrich), *n*-dodecane (Alfa Aesar), dimethyl carbonate (anhydrous, Sigma Aldrich), 2,6-di-*tert*-butylpyridine (DTBP, Thermo Fisher Scientific), *n*-hexane (Fisher), L-carveol (Sigma Aldrich), (+)-limonene-1,2-diol (Sigma Aldrich), and (+)-dihydrocarvone (Sigma Aldrich).

2.2. Catalyst preparation

Bulk phosphotungstic acid (HPW) and phosphomolybdic acid (HPMo) were prepared by drying HPW hydrate and HPMo hydrate, respectively, at 300 °C overnight. Their water content was determined by means of thermogravimetric analysis. 10 wt% HPW supported catalysts were prepared using the incipient wetness method as described in detail elsewhere.[22] Briefly, HPW hydrate was dissolved in ethanol and the ethanol mixture was added dropwise onto SiO_2, TiO_2, and ZrO_2. The resulting slurry was kept at room temperature for 24 h followed by drying at 100 °C for 24 h. Before using, the catalysts were dried at 100 °C for 1 h. 20 wt% HPW/SiO_2 was also prepared to replicate the previous work for limonene oxide isomerization[18,19] but was only used in the initial catalyst screening.

Propylsulfonic acid and arenesulfonic acid-functionalized silica (Pr–SiO_2 and Ar–SiO_2, respectively) were prepared as described elsewhere.[23,24] 4 g of Pluronic 123 was dissolved in 126.3 g of 1.9 M HCl at room temperature under stirring with subsequent heating to 40 °C. TEOS was then added into the mixture and prehydrolyzed for 45 min. The resulting mixtures with a molar composition of 0.0369 TEOS, 0.0041 MPTMS, and 0.0369 H_2O_2 for Pr–SiO_2 and 0.0369 TEOS and 0.0041 CSPTMS for Ar–SiO_2 were stirred for 24 h at 40 °C. Then, the mixtures were aged for 24 h at 100 °C under static conditions. The products were filtered and air-dried at room temperature overnight. The template was removed from the resulting materials by ethanol reflux for 24 h (1.5 g per 400 mL of ethanol). Finally, the samples were filtered and dried at 120 °C overnight. Some of the obtained Pr–SiO_2 were further functionalized with phenyl groups (Pr–SiO_2–ph). Briefly, Pr–SiO_2 (~1.5 g) was suspended in a mixture of PhTMS (0.002 mol) in 150 mL toluene for 4 h. The product was collected and air-dried overnight. Then, it was washed in a Soxhlet extractor with CH_2Cl_2/Et_2O for 24 h. The final product was air-dried overnight. Additional synthesis details can be found elsewhere.[25]

2.3. Characterization

Ion-exchange capacities of the sulfonic acid catalysts (Pr–SiO_2, Pr–SiO_2–ph, Ar–SiO_2, and Nafion NR 50) were determined using 2 M NaCl and 0.05 M TMACl. In a typical experiment, 0.1 g of catalyst was added to 10 g of the ion-exchange solution. The resulting suspension was titrated with 0.01 M NaOH. Temperature-programmed desorption of NH_3 (NH_3 TPD) was performed with 0.1 g of sample from 100 °C to 700 °C at a ramping rate of 5 °C min⁻¹ using a chemisorption instrument (Autochem II 2920, Micromeritics) equipped with a thermal conductivity detector (TCD). NH_3 adsorption was done at 100 °C

for 30 minutes and then purged with He gas for 1 h. A reference TPD was performed with the same procedure using He. The NH_3 chemisorption amount was then calculated by subtracting the He TPD curve from the NH_3 TPD curve. DTBP TPD was performed with 0.01 g of sample using a flow reactor (Tandem micro reactor, Rx-3050TR, Frontier Lab) with an on-line GC-FID (7080B, Agilent). An excess of 0.08 M DTBP in *n*-hexane was injected using a microsyringe into a He feed (25 mL min⁻¹). In a typical run, the reactor with the sample was kept at 130 °C during DTBP injection, followed by holding at the same temperature for 1 h while purging with He (25 mL min⁻¹). Then, the temperature was increased to 550 °C at a ramping rate of 5 °C min⁻¹. A He reference TPD was performed using the same procedure. The DTBP chemisorption amount was calculated by subtracting the He TPD curve from the DTBP TPD curve. The TPD experiments were replicated 2–3 times and the average DTBP uptake values are given in Table 2.

X-ray diffraction (XRD) patterns of the catalysts were recorded with an X-ray diffractometer (D500, Siemens) equipped with a CuKα source (λ = 1.5432 Å) operated at 45 kV and 30 mA. N_2 adsorption and desorption was performed at 77 K using a physisorption instrument (ASAP 2020, Micromeritics). The sample was dehydrated at 100 °C for 12 h under vacuum before measurements. Specific surface area and average pore size were calculated using the Brunauer–Emmett–Teller (BET) and Barrett–Joyner–Halenda (BJH) methods, respectively.

2.4. Limonene oxide isomerization

For initial catalyst screening, a mixture of *cis*-/*trans*-limonene oxide (500 μmol), *n*-dodecane (50 μL, internal standard), dimethyl carbonate (5 mL) and catalyst (mass amount added to give equivalent acid site loading of 50 μmol) was intensely stirred under air at room temperature in a 10 mL glass reactor. For detailed screening at low conversion, a mixture of limonene oxide (250 μmol), dodecane (50 μL, internal standard), dimethyl carbonate (3 mL) and catalyst sample was vigorously stirred under air at 5 °C in a 10 mL glass reactor. The catalyst loading was varied to achieve 13–15% conversion. The catalyst loading used for these conversion levels are given in the ESI.† The reaction mixture was sampled at a reaction time of 15 min, followed by filtering of the solid catalyst using a syringe filter. The filtered reaction mixture was analyzed using a gas chromatograph (GC, 7890A, Agilent) equipped with an FID and mass spectrometer (5975C, Agilent). Calibration was performed using commercial chemicals except for 1-methyl-3-(prop-1-en-2-yl) cyclopentane-1-carbaldehyde, as it is not commercially available. Identification of the aldehyde reaction product is described in the ESI.† Details on the calculation of the conversion and selectivity are given in the ESI.†

3. Results and discussion

3.1. Catalyst screening

The initial catalyst testing was performed to screen the relative importance of acid catalyst properties on limonene oxide

5320 | *Catal. Sci. Technol.*, 2025, **15**, 5318–5326

This journal is © The Royal Society of Chemistry 2025

Table 1 Limonene oxide isomerization with solid acids (conditions: 22 °C, catalyst acid site loading 50 μmol, limonene oxide 500 μmol, dimethyl carbonate 5 mL)

Catalyst	Reaction time (min)	Conversion of limonene oxide (%)	Dihydrocarvone yield (%)	Dihydrocarvone selectivity (%)	Carbon balance
Pr–SiO$_2$	300	94	26	28	60
Pr–SiO$_2$–ph	300	87	28	33	70
Ar–SiO$_2$	10	96	14	15	62
Nafion NR50	10	10	6	66	99
20 wt% HPW/SiO$_2$	10	100	68	68	81

isomerization. In addition to acid strength, the impact of catalyst surface hydrophilicity was examined since hydrophilic silica-supported phosphotungstic acid (HPW/SiO$_2$) showed a high reaction rate and selectivity to dihydrocarvone in previous studies.[18,19] Five types of catalysts (Table 1) with different hydrophilicity/hydrophobicity and acid strength were included in the initial screening, which included Nafion NR50, HPW/SiO$_2$, propylsulfonic acid-functionalized SiO$_2$ catalysts with and without functionalized phenyl groups (Pr–SiO$_2$ and Pr–SiO$_2$–ph) and an arenesulfonic acid-functionalized SiO$_2$ catalyst (Ar–SiO$_2$). With respect to acid strength, Nafion NR50 is reported to be super acidic[26] and the acid strength of the other catalysts are expected to decrease in the order: HPW/SiO$_2$ ≫ Ar-SiO$_2$ > Pr–SiO$_2$. Regarding hydrophilicity, HPW/SiO$_2$, Pr–SiO$_2$ and Ar–SiO$_2$ are hydrophilic, while Pr–SiO$_2$–ph with phenyl groups is less hydrophilic. Also, Nafion NR50 has acid sites branched from hydrophobic polymer chains, thus, making it hydrophobic.

With the same acid site loading, Nafion NR50 and HPW/SiO$_2$, which have high acid strength, showed higher selectivity to dihydrocarvone (66–68%) regardless of their hydrophobicity/hydrophilicity as shown in Table 1. Also, Pr–SiO$_2$–ph with hydrophobic phenyl groups showed similar dihydrocarvone selectivity (33%) to Pr–SiO$_2$ without the phenyl groups (28%). These results suggested that the effect of acid strength on dihydrocarvone selectivity was significant while the effect of hydrophilicity/hydrophobicity was not significant. Furthermore, HPW/SiO$_2$ and Ar–SiO$_2$ showed almost complete conversion in a reaction time of 10 min, while about 300 min was required for Pr–SiO$_2$ to reach ~90% conversion. These results indicated that the catalytic activity depended on the catalyst acid strength, as reported in various acid-catalyzed systems.[27–29] However, the Nafion catalyst with high acid strength showed relatively low activity, which is likely due to its high hydrophobicity inhibiting swelling in the solvent thereby preventing reactant access to internal acid sites.

3.2. Acidity characterization of four types of solid acids

Given the apparent strong influence of Brønsted acid strength on the activity of the limonene oxide isomerization reaction as well as selectivity to dihydrocarvone, more detailed screening and characterization were performed on the heteropoly acid and sulfonic acid catalysts including bulk phosphotungstic acid (bulk HPW), bulk phosphomolybdic acid (bulk HPMo), and arenesulfonic and propylsulfonic-acid functionalized SiO$_2$ (Ar–

SiO$_2$ and Pr–SiO$_2$). The relative acid strength of the catalysts was first compared using NH$_3$ TPD, as shown in Fig. 1. The desorption temperatures of ammonia were identified by comparing curves obtained with and without the probe molecule (Fig. S1†), as increasing the catalyst temperature can result in sample decomposition or water removal. The sulfonic acid catalyst peaks at high temperatures (350–650 °C) are attributed to decomposition of the catalysts instead of ammonia desorption, as the peaks were observed in the absence of the titrant. While it might be expected that organosulfonic acid catalysts possess a narrow acid strength range due to their well-defined structure, broad NH$_3$ desorption peaks were obtained, which was consistent with previous studies.[30–32] This result indicates that acidity characterization techniques involving TPD methodology may not be ideal for the organosulfonic acid catalysts as NH$_3$ may be trapped in micropores of the organosulfonic acid catalysts. The presence of micropores was confirmed by N$_2$ adsorption–desorption isotherms (Fig. S2†), which can lead to TPD peak broadening. In the case of bulk HPAs, NH$_3$ trapping would not be significant given their low porosity (Table S1 and Fig. S2†), which is consistent with the observed narrow acid strength ranges. A concern with TPD is that desorbed probe molecules can also readsorb on non-acid sites on their way out of the pores, complicating the acidity analysis.[33,34] However, NH$_3$ readsorption in HPAs was only observed under high pressure of NH$_3$ at temperatures below room temperature.[35] While comparing the acid strength of microporous materials, including zeolites, using a TPD technique can be complicated due to desorbed molecule trapping or readsorption in micropores; this concern is
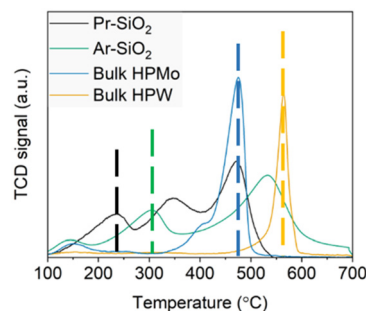

Fig. 1 NH$_3$ TPD of solid acids (chemisorption 100 °C, NH$_3$ desorption temperatures (marked in dashed lines) were obtained considering catalyst decomposition and water removal).

Table 2 Acid site densities of the catalysts (2,6-di-*tert*-butyl pyridine: DTBP)

Catalyst	Ion-exchanged proton density (μmol g^{-1})	NH$_3$ uptake (μmol g^{-1})	DTBP uptake (μmol g^{-1})
Pr–SiO$_2$	960	—	307 ± 10
Ar–SiO$_2$	1070	—	481 ± 66
Bulk HPMo	—	2446 ± 50	18 ± 4
Bulk HPW	—	1052 ± 15	33 ± 12
10 wt% HPW/SiO$_2$	—	—	87 ± 3
10 wt% HPW/TiO$_2$	—	—	59 ± 2
10 wt% HPW/ZrO$_2$	—	—	31 ± 2

mitigated for the case of mesoporous catalysts or bulk catalysts with low porosity. According to the NH$_3$ TPD results, the acid strength was observed to decrease in the expected order: bulk HPW > bulk HPMo > Ar–SiO$_2$ > Pr–SiO$_2$.

Acid site densities were measured employing conventional methods for the type of catalyst as well as 2,6-di-*tert*-buytl pyridine (DTBP) chemisorption (Table 2). The acid site density values for the bulk heteropoly acids were investigated by means of chemisorption, with both NH$_3$ and DTBP used as the titrant. As the goal of the acid site measurement was to determine the number of protons accessible in the reaction system of interest, the larger DTBP titrant was compared to that obtained using NH$_3$ given the size of the limonene oxide molecule. The measured NH$_3$ uptake of the bulk HPW (1052 μmol g$_{cata}^{-1}$) and bulk HPMo (2446 μmol g$_{cata}^{-1}$) were similar to the mass-based proton values calculated just using their molecular formulas leading to 1032 μmol g$_{cata}^{-1}$ and 1644 μmol g$_{cata}^{-1}$, respectively. The agreement between these values affirmed that NH$_3$ chemisorption provided titration of the protons through the bulk of the heteropoly acid materials. The results were consistent with a previous study in which NH$_3$ titration of bulk protons in heteropoly acids was demonstrated gravimetrically.[35] Brønsted acidic HPW[36] showed NH$_3$ uptake close to its mass-based proton density. However, the NH$_3$ uptake for bulk HPMo (2446 μmol g$_{cata}^{-1}$) was larger than the mass-based proton density (1644 μmol g$_{cata}^{-1}$), which suggested that bulk HPMo possess Lewis acid sites. This result is consistent with that reported by Pedada *et al.*[37] in which the presence of Lewis acidic sites for HPMo was demonstrated by means of adsorbed pyridine infrared experiments. Lewis acidity of bulk HPMo may be attributed to oxides such as P$_2$O$_5$ and MoO$_3$, which are formed as Keggin units that are deconstructed during dehydration.[38]

DTBP was used to characterize surface proton sites of HPAs. DTBP has been used to characterize external Brønsted acidity of zeolites[39] as well as supported heteropoly acids,[40–42] as its large kinetic diameter (0.79 nm) prevents titration of acid sites within the micropores. DTBP titrates just Brønsted acid sites, as its butyl groups hinder interaction with Lewis acid sites. Additionally, NH$_3$ and pyridine have been shown not to selectively characterize just the surface acid sites of heteropoly acids but also to access bulk acid sites in HPAs.[35,43] Notably, the bulk heteropoly acids showed DTBP uptake of about 1–3% of their NH$_3$ chemisorption values (Table 2). The values obtained with DTBP were similar to that calculated for geometric surface proton densities, 24 μmol g$_{cata}^{-1}$ and 13 μmol g$_{cata}^{-1}$ for bulk HPW and bulk HPMo, respectively. The calculated values were determined using the cross-sectional area of a Keggin unit (144 Å^2)[27] and the measured surface areas of the bulk HPW and bulk HPMo (Table S1†). Therefore, as with zeolites, the DTBP chemisorption seemed to only titrate surface protons. The significant difference between the NH$_3$ and DTBP chemisorption results suggests that the number of active sites for heteropoly acid catalysts should be determined by considering the proton accessibility for the reactant, which will depend on the reaction system. Given the molecular size of limonene oxide, DTBP chemisorption was used for active site density measurement in calculating the reaction turnover rate.

Proton density values for the organosulfonic acid catalysts were investigated by means of conventional proton exchange and DTBP chemisorption. First, the proton density was obtained by proton exchange followed by titration, as they possess proton-exchange capacity. The obtained proton densities for Pr–SiO$_2$ and Ar–SiO$_2$ were within 13% and 4% differences, respectively, from the reported concentrations in the literature for the synthesis recipe used.[24,44] The measured DTBP uptake for the organosulfonic acid catalysts was lower than the values obtained from proton exchange. This difference is likely due to acid sites in micropores that DTBP could not access (Fig. S2†). As DTBP is more like the molecular size of limonene oxide, DTBP uptake values were used as the accessible active site density in calculating the reaction turnover rate.

3.3. Effect of acid strength on limonene oxide isomerization

Limonene oxide isomerization results with catalysts possessing different acid strength under the same reaction conditions and comparable conversion levels are shown in Fig. 2. A target conversion of 13–15% was used to allow for direct comparison of the turnover rate and selectivity. *cis*-Limonene oxide was more reactive than *trans*-limonene oxide for all catalysts, as the *cis*-/*trans*- ratio (0.74) decreased after reaction, which is consistent with a previous study.[19,20] Notably, the relative reactivity of *cis*- and *trans*-limonene oxide didn't depend on the type of catalyst, as the post-reaction *cis*-/*trans*-limonene oxide ratio was similar for all the catalysts (0.53–0.58). Bulk HPW, which has the highest acid strength, showed a 170-fold higher turnover rate than Pr–SiO$_2$, which has the lowest acid strength (Fig. 2a). Notably, dihydrocarvone selectivity also increased

5322 | *Catal. Sci. Technol.*, 2025, **15**, 5318–5326

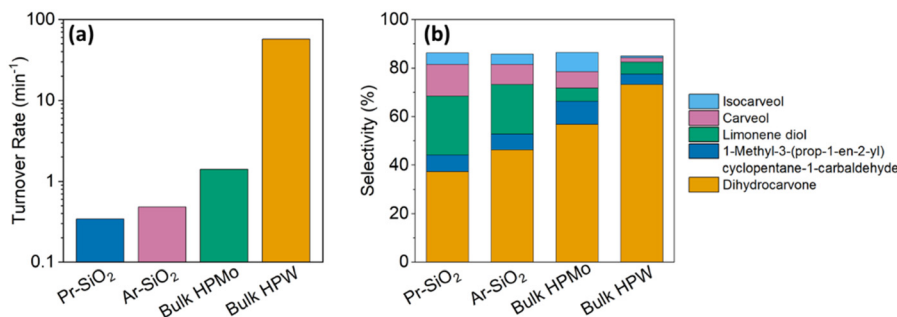This journal is © The Royal Society of Chemistry 2025

Fig. 2 Limonene oxide isomerization turnover rates (a) and selectivity distribution (b) of the solid acids (conditions: 5 °C, conversion 13–15%, reaction time 15 min, limonene oxide 225 μmol, dimethyl carbonate 3 mL, DTBP uptake used for turnover rate calculation).

significantly with increasing catalyst acid strength (Fig. 2b). For all catalysts, the major product was dihydrocarvone, but the dihydrocarvone selectivity ranged from 37–73% (Fig. 2b). Limonene oxide isomers such as carveol, isocarveol, and 1-methyl-3-(prop-1-en-2-yl)cyclopentane-1-carbaldehyde, as well as limonene diol, were observed as by-products. Limonene diol is produced from the hydration of limonene oxide. The sulfonic acid catalysts (Pr–SiO$_2$ and Ar–SiO$_2$) showed relatively higher limonene diol selectivity. A high carbon balance (98–99%) was found for the reaction results shown in Fig. 2, which were higher than those shown in Table 1, as the reaction conditions employed in the former largely suppressed limonene oxide oligomerization.

To investigate the effect of acid strength, both ammonia and DTBP desorption temperatures were used. Fig. 3a shows the positive correlation of the turnover rate and NH$_3$ desorption temperature. Importantly, no correlation between acid strength and the turnover rate was found if the NH$_3$ chemisorption results were used to quantify total acid sites for the bulk heteropoly acids. This result suggests that bulk protons in the heteropoly acids do not catalyze limonene oxide isomerization. Further, the relationship between acid strength and dihydrocarvone selectivity is shown in Fig. 3b, where there was also a positive correlation between acid strength and dihydrocarvone selectivity. As bulk HPW showed the highest activity and dihydrocarvone selectivity, further work was performed to determine the effect of supporting

HPW on different metal oxides so as to maximize the number of available acid sites for HPW, *i.e.*, higher dispersion of HPW. The relationship of limonene oxide isomerization and acid strength represented by the DTBP desorption temperature is further discussed, including the supported HPW catalysts, in section 3.5.

3.4. Characterization for HPW catalysts

Bulk HPW and HPW supported on neutral SiO$_2$, acidic TiO$_2$, and amphoteric ZrO$_2$ were also studied. Fig. 4 shows XRD patterns for the bulk and supported HPW catalysts. HPW/SiO$_2$ showed peaks characteristic of the Keggin structure for HPW indicating the existence of small HPW clusters. HPW/TiO$_2$ and HPW/ZrO$_2$ showed peaks attributed to the support only, which was likely due to the high crystallinity of titania and zirconia.

Surface acid sites of supported HPW were characterized by means of DTBP chemisorption. DTBP uptake values of the catalysts are shown in Table 2. Though metal oxide supports possess surface hydroxyl groups, which can act as a weak Brønsted acid site, they are not titrated by DTBP due to the relatively weak basicity of DTBP. Also, the SiO$_2$, TiO$_2$, and ZrO$_2$ supports were not active under the reaction conditions. The DTBP uptake of 10 wt% HPW/SiO$_2$ and HPW/TiO$_2$ was about 2–3 times higher compared to bulk HPW due to the dispersion of phosphotungstic acid on the supports. HPW supported on silica
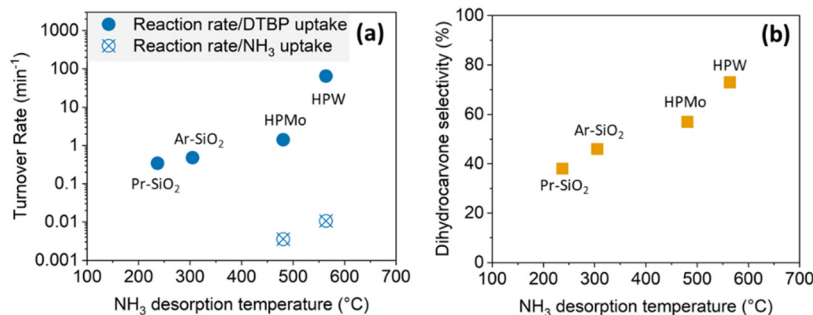

Fig. 3 Correlation of NH$_3$ desorption temperature to turnover rate (a) and dihydrocarvone selectivity (b) for solid acids (conditions: 5 °C, conversion 13–15%, reaction time 15 min, limonene oxide 225 μmol, dimethyl carbonate 3 mL, turnover rate calculated using the DTBP uptake (●) and NH$_3$ uptake (⊗)).
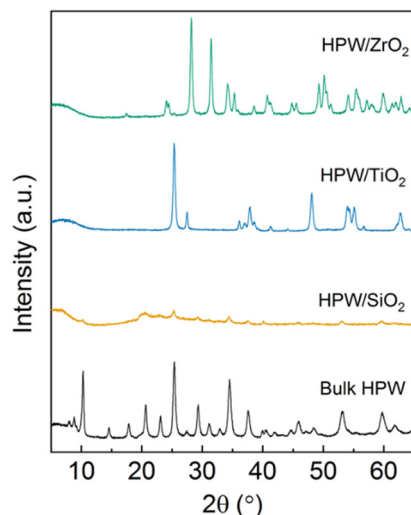
Fig. 4 XRD spectra of the heteropoly acid catalysts.

Fig. 5 DTBP TPD of HPW catalysts (catalyst 0.01 g, 0.08 M DTBP in *n*-hexane, chemisorption 130 °C).

showed DTBP uptake (87 μmol g_{cata}^{-1}) lower than mass-based proton density (104 μmol g_{cata}^{-1}). As the existence of HPW clusters on the silica was confirmed by XRD (Fig. 4), this difference can be attributed to inaccessible acid sites in the HPW clusters. The lower DTBP uptake for HPW/TiO$_2$ (59 μmol g_{cata}^{-1}) and HPW/ZrO$_2$ (31 μmol g_{cata}^{-1}) could be due to the presence of HPW aggregates given the low surface areas of the supports. As a surface area of at least 30 m^2 g^{-1} is needed to form an HPW monolayer in a 10 wt% HPW catalyst, ZrO$_2$ (22 m^2 g^{-1}) and TiO$_2$ (49 m^2 g^{-1}) would not provide sufficient surface area for complete dispersion of HPW on the supports[31] P NMR results (Fig. S3†) support the existence of HPW aggregates for the HPW/TiO$_2$ and HPW/ZrO$_2$. As the interaction between HPW and supports decreases in the following order: HPW/SiO$_2$ > HPW/TiO$_2$ > HPW/ZrO$_2$ as demonstrated by observations from DRIFT and X-ray spectroscopic data,[36] the phosphorous chemical shift values from[31] P NMR decreased in the same order[22,45] when HPW is dispersed. However, the chemical shifts for HPW/TiO$_2$ and HPW/ZrO$_2$ (Fig. S3†) were higher than for HPW/SiO$_2$, suggesting the existence of bigger HPW clusters on TiO$_2$ and ZrO$_2$. Using the same rationale discussed in section 3.3, the DTBP uptake was used as the active site density for calculating the reaction turnover rate for the supported HPW catalysts.

While NH$_3$ TPD was problematic for determining the number of accessible catalytic sites, it did appear to be effective in characterizing acid strength of the sites as discussed in section 3.2. However, for the supported heteropoly acid catalysts, comparison of the TPD profiles with and without NH$_3$ did not provide clear characterization due to the lack of distinct NH$_3$ signals (Fig. S4†). To confirm the consistency of the DTBP desorption results with the NH$_3$ results given in the previous section, DTBP TPD profiles of bulk HPW, bulk HPMo and sulfonic acid catalysts were compared as shown in Fig. S5.† The acid strength was observed to decrease in the order: bulk HPW ≫ bulk HPMo > Ar–SiO$_2$ > Pr–SiO$_2$, which was consistent with the order from NH$_3$ TPD.
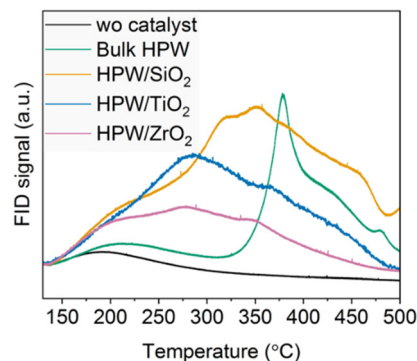
The surface acid strength for bulk and supported HPW catalysts was investigated using DTBP TPD as shown in Fig. 5. Desorption temperatures of DTBP were identified by comparing curves obtained with and without the probe molecule (Fig. S6†). The acid strength was observed to decrease in the order: bulk HPW > HPW/SiO$_2$ > HPW/TiO$_2$ > HPW/ZrO$_2$. As phosphotungstic acid is dispersed on supports, acid strength decreased due to interaction between the support and phosphotungstic acid. Given the larger HPW aggregates on HPW/ZrO$_2$ and HPW/TiO$_2$ than HPW/SiO$_2$, further reduction in acid strength for HPW/ZrO$_2$ and HPW/TiO$_2$ indicates strong interaction of HPW and the supports. Notably, the acid strength order for the materials was consistent with the order obtained using ammonia adsorption heat, a technique which is commonly used to characterize supported and bulk heteropoly acids.[36] While the NH$_3$ heat of adsorption allowed comparing acid strength with a single value, DTBP TPD provided information on the distribution of acid site strength.

3.5. Effect of acid strength of HPA catalysts on limonene oxide isomerization

Limonene oxide isomerization results with various HPW catalysts under the same reaction conditions are shown in Fig. 6. A target conversion of 13–15% was used. When HPW was supported, the reaction rate decreased, and the bulk HPW showed the highest reaction rate (Fig. 6a). Also, dihydrocarvone selectivity slightly decreased when HPW was supported. However, dihydrocarvone was a major product for all the HPW catalysts with 67–73% dihydrocarvone selectivity.

The correlation of the DTBP desorption temperature to the turnover rate and the dihydrocarvone selectivity is shown in Fig. 7. Organosulfonic acid catalysts and bulk HPMo possessing weaker acid strength than HPW catalysts were included to see the correlations in a boarder range of acid strengths. Positive correlations of surface acid strength to catalytic activity and dihydrocarvone selectivity were observed. As the catalysts possess a wide range of porosities (surface area 4–516 m^2 g$_{cata}^{-1}$) and HPW is supported on different surfaces, the correlations indicate that acid strength is a key factor dictating the reaction rate and selectivity of
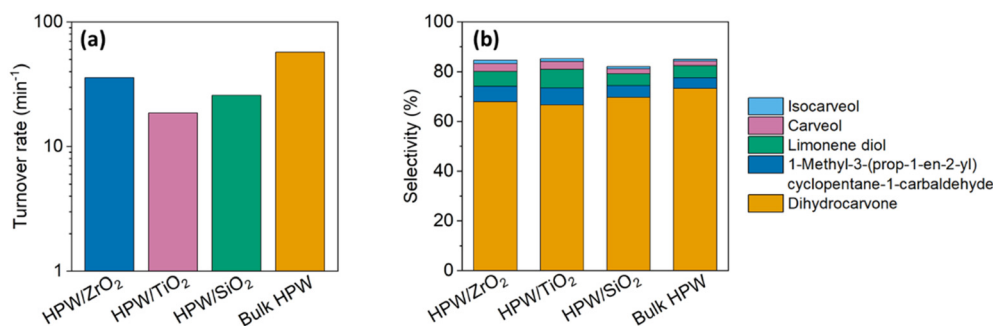
5324 | *Catal. Sci. Technol.*, 2025, **15**, 5318–5326

This journal is © The Royal Society of Chemistry 2025

Fig. 6 Limonene oxide isomerization turnover rates (a) and selectivity distribution (b) of HPW catalysts (conditions: 5 °C, conversion 13–15%, reaction time 15 min, limonene oxide 225 μmol, dimethyl carbonate 3 mL, DTBP uptake used for turnover rate calculation).

limonene oxide isomerization. Considering that limonene oxide can be converted into various isomers, including carveol, isocarveol, 1-methyl-3-(prop-1-en-2-yl)-cyclopentane-1-carbaldehyde, and dihydrocarvone, and limonene diol over a Brønsted acid catalyst, as the reaction network proposed by Costa *et al.*,[18] the relationship between acid strength and dihydrocarvone selectivity suggests that the activation energy for dihydrocarvone formation can be higher than the other reaction pathways.

4. Conclusions

In this work, limonene oxide isomerization has been studied with a wide range of Brønsted acid catalysts, which included heteropoly acids (HPAs) and organosulfonic acids. Accessible acid site density and surface acid strength of the catalysts was investigated by means of 2,6-di-*tert*-butylpyridine (DTBP) temperature-programmed desorption. A clear correlation between the turnover rate calculated using DTBP chemisorption amount and surface acid strength represented by DTBP desorption temperature was obtained, thereby validating the chemisorption technique. Phosphotungstic acid catalysts demonstrated much higher catalytic activities and dihydrocarvone selectivity than sulfonic acid catalysts, which

correlated with high Brønsted acid strength. Strong relationships between the turnover rate and acid strength, represented by desorption temperatures of ammonia and DTBP, were obtained for all of the catalysts. Further, a positive correlation of acid strength and dihydrocarvone selectivity was also established. These correlations show catalytic activity and dihydrocarvone selectivity are dictated by catalyst acid strength, regardless of the catalyst porosity and support surfaces.

Data availability

The authors confirm that the data supporting the findings of this study are available within the article and its ESI.†

Author contributions

Hyunju Lee designed and performed experiments and analysed the experimental results. She also led the writing of the manuscript. Hsi-Hsin Lin proposed the investigation of the acid strength effect on limonene oxide isomerization and conceptualized/drew the limonene star diagram. Brent H. Shanks guided the project and revised the manuscript.

Conflicts of interest

There are no conflicts to declare.

Acknowledgements

Fig. 7 Correlation of DTBP desorption temperature to the turnover rate and dihydrocarvone selectivity for solid acid catalysts: (1) Pr–SiO₂, (2) Ar–SiO₂, (3) bulk HPMo, (4) HPW/ZrO₂, (5) HPW/TiO₂, (6) HPW/SiO₂, and (7) bulk HPW (Conditions: 5 °C conversion 13–15%, reaction time 15 min, limonene oxide 225 μmol, dimethyl carbonate 3 mL, DTBP uptake used for turnover rate calculation).

Notes and references

1 I. V. Kozhevnikov, *Chem. Rev.*, 1998, **98**, 171–198.
2 M. N. Timofeeva, *Appl. Catal., A*, 2003, **256**, 19–35.
3 M. Sun, J. Zhang, P. Putaj, V. Caps, F. Lefebvre, J. Pelletier and J.-M. Basset, *Chem. Rev.*, 2014, **114**, 981–1019.
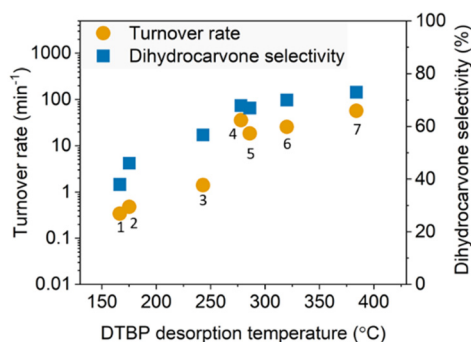
4 N. L. Z. Z. Adil, T. S. T. Saharuddin, L. N. Ozair and F. W. Harun, *IOP Conf. Ser.:Mater. Sci. Eng.*, 2021, **1173**, 012073.

5 L. Hombach, N. Simitsis, J. T. Vossen, A. J. Vorholt and A. K. Beine, *ChemCatChem*, 2022, **14**, e202101838.

6 E. Louisy, V. Khodyrieva, S. Olivero, V. Michelet and A. Mija, *ChemPlusChem*, 2022, **87**, e202200190.

7 A. Satira, C. Espro, E. Paone, P. S. Calabrò, M. Pagliaro, R. Ciriminna and F. Mauriello, *Catalysts*, 2021, **11**, 387.

8 E. Jongedijk, K. Cankar, M. Buchhaupt, J. Schrader, H. Bouwmeester and J. Beekwilder, *Appl. Microbiol. Biotechnol.*, 2016, **100**, 2927–2938.

9 K. Januszewicz, P. Kazimierski, W. Kosakowski and W. M. Lewandowski, *Materials*, 2020, **13**, 1359.

10 Limonene Market Size, Share & Trends Analysis Report By Source (Orange, Mandarin, Grapefruit), By End-Use (Personal Care Products, Food Products), By Region, And Segment Forecasts, 2023–2030.

11 C. S. Graebin, M. de F. Madeira, J. K. U. Yokoyama-Yasunaka, D. C. Miguel, S. R. B. Uliana, D. Benitez, H. Cerecetto, M. González, R. G. da Rosa and V. L. Eifler-Lima, *Eur. J. Med. Chem.*, 2010, **45**, 1524–1528.

12 M. R. Thomsett, J. C. Moore, A. Buchard, R. A. Stockman and S. M. Howdle, *Green Chem.*, 2019, **21**, 149–156.

13 B. H. H. Goh, C. T. Chong, H. C. Ong, T. Seljak, T. Katrašnik, V. Józsa, J.-H. Ng, B. Tian, S. Karmarkar and V. Ashokkumar, *Energy Convers. Manage.*, 2022, **251**, 114974.

14 B. H. Shanks and P. L. Keeling, *Green Chem.*, 2017, **19**, 3177–3185.

15 L. Zhang, G. Fan, X. Li, J. Ren, W. Huang, S. Pan and J. He, *J. Sci. Food Agric.*, 2022, **102**, 3297–3307.

16 Y. Dong, K. J. McCullough, S. Wittlin, J. Chollet and J. L. Vennerstrom, *Bioorg. Med. Chem. Lett.*, 2010, **20**, 6359–6361.

17 H.-P. J. De Rouville, G. Vives, E. Tur, J. Crassous and G. Rapenne, *New J. Chem.*, 2009, **33**, 293–299.

18 V. V. Costa, K. A. da Silva Rocha, I. V. Kozhevnikov, E. F. Kozhevnikova and E. V. Gusevskaya, *Catal. Sci. Technol.*, 2013, **3**, 244–250.

19 R. F. Cotta, R. A. Martins, M. M. Pereira, K. A. da Silva Rocha, E. F. Kozhevnikova, I. V. Kozhevnikov and E. V. Gusevskaya, *Appl. Catal., A*, 2019, **584**, 117173.

20 A. Rejzková and E. Vyskočilová, *React. Kinet., Mech. Catal.*, 2025, **138**, 47–69.

21 J. E. Sánchez-Velandia and A. L. Villa, *Catal. Today*, 2021, **394–396**, 208–218.

22 Y. P. Wijaya, H. P. Winoto, Y.-K. Park, D. J. Suh, H. Lee, J.-M. Ha and J. Jae, *Catal. Today*, 2017, **293–294**, 167–175.

23 D. Margolese, J. A. Melero, S. C. Christiansen, B. F. Chmelka and G. D. Stucky, *Chem. Mater.*, 2000, **12**, 2448–2459.

24 G. Morales, M. Paniagua, J. A. Melero, G. Vicente and C. Ochoa, *Ind. Eng. Chem. Res.*, 2011, **50**, 5898–5906.

25 I. Mbaraka and B. Shanks, *J. Catal.*, 2005, **229**, 365–373.

26 Y. Chang, C. Lee and C. Bae, *RSC Adv.*, 2014, **4**, 47448–47454.

27 W. Alharbi, E. F. Kozhevnikova and I. V. Kozhevnikov, *ACS Catal.*, 2015, **5**, 7186–7193.

28 W. Knaeble and E. Iglesia, *J. Catal.*, 2016, **344**, 817–830.

29 W. Knaeble, R. T. Carr and E. Iglesia, *J. Catal.*, 2014, **319**, 283–296.

30 A. A. Dabbawala, J. J. Park, A. H. Valekar, D. K. Mishra and J.-S. Hwang, *Catal. Commun.*, 2015, **69**, 207–211.

31 M. A. Naik, D. Sachdev and A. Dubey, *Catal. Commun.*, 2010, **11**, 1148–1153.

32 L. Saikia, J. Satyarthi, D. Srinivas and P. Ratnasamy, *J. Catal.*, 2007, **252**, 148–160.

33 C.-A. Trujillo, N.-T. Ramírez-Marquez and J.-S. Valencia-Rios, *Thermochim. Acta*, 2020, **689**, 178651.

34 Miki Niwa, Naonobu Katada and Kazu Okumura, *Characterization and Design of Zeolite Catalysts: Solid Acidity, Shape Selectivity and Loading Properties*, Springer, 2010.

35 A. Micek-Ilnicka and B. Gil, *Vib. Spectrosc.*, 2007, **43**, 435–439.

36 A. Alasmari, R. Al-Faze, E. F. Kozhevnikova and I. V. Kozhevnikov, *Catal. Commun.*, 2023, **180**, 106710.

37 J. Pedada, H. B. Friedrich and S. Singh, *Catal. Lett.*, 2018, **148**, 1355–1365.

38 S. Kendell and T. Brown, *React. Kinet., Mech. Catal.*, 2010, **99**, 251–268.

39 K. Góra-Marek, K. Tarach and M. Choi, *J. Phys. Chem. C*, 2014, **118**, 12266–12274.

40 R. T. Carr, M. Neurock and E. Iglesia, *J. Catal.*, 2011, **278**, 78–93.

41 W. Knaeble and E. Iglesia, *J. Phys. Chem. C*, 2016, **120**, 3371–3389.

42 R. Al-Faze, A. Finch, E. F. Kozhevnikova and I. V. Kozhevnikov, *Appl. Catal., A*, 2020, **597**, 117549.

43 B. Hodnett, *J. Catal.*, 1984, **88**, 253–263.

44 J. A. Melero, L. F. Bautista, G. Morales, J. Iglesias and R. Sánchez-Vázquez, *Chem. Eng. J.*, 2010, **161**, 323–331.

45 A. M. Alsalme, P. V. Wiper, Y. Z. Khimyak, E. F. Kozhevnikova and I. V. Kozhevnikov, *J. Catal.*, 2010, **276**, 181–189.

5326 | *Catal. Sci. Technol.*, 2025, **15**, 5318–5326

This journal is © The Royal Society of Chemistry 2025